

Enhancement of Performance and Mechanism Studies of All-Solution Processed Small-Molecule based Solar Cells with an Inverted Structure

Guankui Long,^{†,||} Bo Wu,^{‡,||,⊥} Xuan Yang,[†] Bin Kan,[†] Ye-cheng Zhou,[§] Li-chuan Chen,[§] Xiangjian Wan,[†] Hao-li Zhang,[§] Tze Chien Sum,^{*,‡} and Yongsheng Chen^{*,†}

[†]State Key Laboratory and Institute of Elemento-Organic Chemistry and Centre for Nanoscale Science and Technology, Institute of Polymer Chemistry and Collaborative Innovation Center of Chemical Science and Engineering (Tianjin), College of Chemistry, Nankai University, Tianjin, 300071, China

[‡]Division of Physics and Applied Physics, School of Physical and Mathematical Sciences, Nanyang Technological University, 21 Nanyang Link, 637371, Singapore

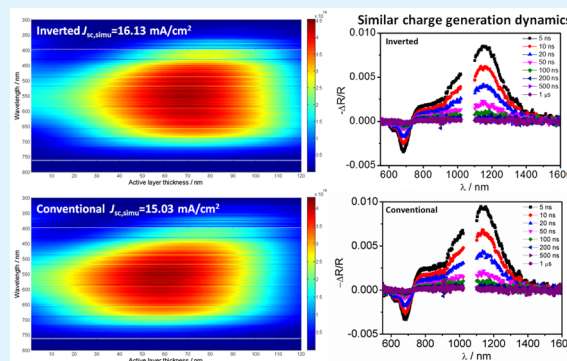
[§]State Key Laboratory of Applied Organic Chemistry (SKLAOC), College of Chemistry and Chemical Engineering, Lanzhou University, Lanzhou, 730000, China

[⊥]Singapore-Berkeley Research Initiative for Sustainable Energy (SinBerISE), 1 Create Way, Singapore 138602, Singapore

Supporting Information

ABSTRACT: Both solution-processed polymers and small molecule based solar cells have achieved PCEs over 9% with the conventional device structure. However, for the practical applications of photovoltaic technology, further enhancement of both device performance and stability are urgently required, particularly for the inverted structure devices, since this architecture will probably be most promising for the possible coming commercialization. In this work, we have fabricated both conventional and inverted structure devices using the same small molecular donor/acceptor materials and compared the performance of both device structures, and found that the inverted structure based device gave significantly improved performance, the highest PCE so far for inverted structure based device using small molecules as the donor. Furthermore, the inverted device shows a remarkable stability with almost no obvious degradation after three months. Systematic device physics and charge generation dynamics studies, including optical simulation, light-intensity-dependent current–voltage experiments, photocurrent density-effective voltage analyses, transient absorption measurements, and electrical simulations, indicate that the significantly enhanced performance using inverted device is ascribed to the increasing of J_{sc} compared to the conventional device, which in turn is mainly attributed to the increased absorption of photons in the active layers, rather than the reduced nongeminate recombination.

KEYWORDS: organic photovoltaic, small molecules, inverted device, transient absorption spectra, electrical simulation



1. INTRODUCTION

Solution processed solar cells have received great research interests as a clean and competitive renewable energy source due to their attractive features such as low-cost, lightweight, solution processability, high mechanical flexibility, rapid energy payback time, and so forth.^{1–4} According to the charge transport directions, organic photovoltaics (OPVs) could be divided into conventional and inverted device structures,^{5,6} where the inverted structure based devices are most likely the case for the final commercial applications.⁷ Since the report for the first inverted device in 2005,⁸ great progress has been made,^{9–14} and recently, the PCE for polymer-based OPV (P-OPV) have improved to over 9% by several groups with inverted structure devices.^{15–19}

Meanwhile, small molecule based OPVs (SM-OPVs) have also stimulated great attention,^{20–24} owing to its well-defined molecular structures, intrinsic monodispersity, high purity, less batch to batch variation, more easily controlled energy levels, absorption and so forth,^{25–45} compared with the P-OPVs. Very recently, the PCE for conventional SM-OPV devices has reached over 9%.^{27,35,46} However, for the more commercial-related inverted devices with generally higher stability, the much deserved attention for SM-OPVs is not forthcoming. Hence, little is known about the device structure and

Received: June 16, 2015

Accepted: September 9, 2015

Published: September 9, 2015

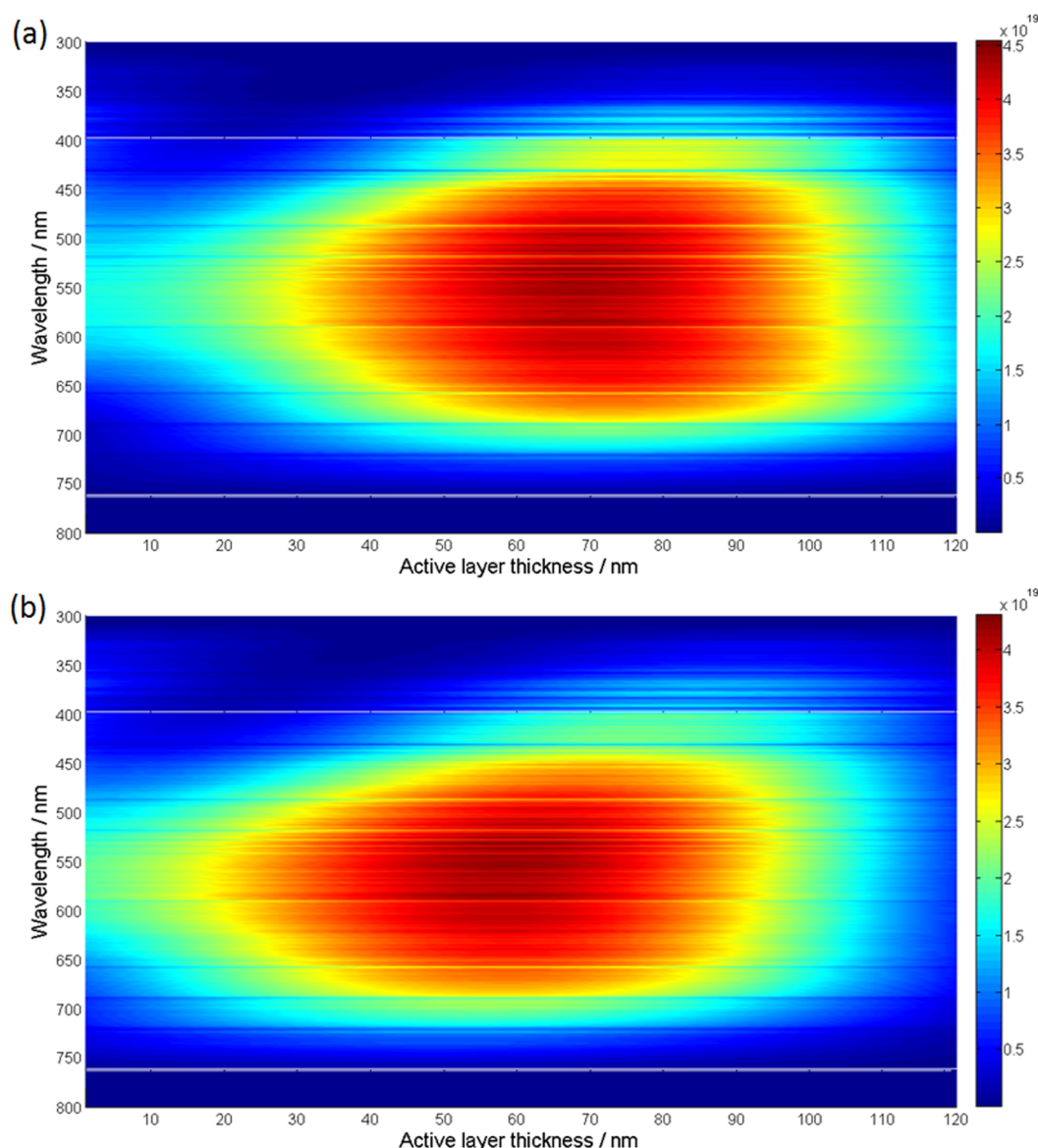


Figure 2. Simulated exciton generation rates in the studied inverted device (a) and conventional device (b) as a function of depth of the active layer calculated using a one-dimensional transfer matrix model. The incidence light entered the device from the left of the Figure (0 nm at the x -axis).

2.4. Light Intensity Experiment. In order to investigate the dependence of V_{oc} and J_{sc} on the light intensity, the intensity of the light was modulated with a series of two neutral density filters wheels of six filters apiece, allowing for up to 17 steps to adjust the intensity from 100 to 5 mW cm⁻².

2.5. Transient Absorption Spectroscopy. Transient absorption measurements were performed using a commercial Helios and EOS setups (Ultrafast Systems LLC). They were used to measure transient absorption dynamics in the fs–ns and ns– μ s time regimes, respectively. The pump pulse (500 nm) was generated from an optical parametric amplifier (OPerA Solo) that was pumped by a 1-kHz regenerative amplifier (Coherent Libra). The beam from the regenerative amplifier has a center wavelength at 800 nm, a pulse width of around 50 fs, and a power of 4 mJ per pulse. The regenerative amplifier was seeded by a mode-lock Ti:sapphire oscillator (Coherent Vitesse, 80 MHz). The pump beam energy was set to be around 15 μ J/cm² per pulse. The probe beam for Helios was a white light continuum generated from either a 2 mm sapphire plate for the visible part (400–800 nm) or a 1 cm sapphire plate for the NIR part (800 nm–1600 nm) using the 800 nm fundamental from the regenerative amplifier above. The probe beam for EOS was a white continuum generated from a photonic fiber using a Nd:YAG laser (center

wavelength: 1064 nm). The probe beam was collected using a dual detector for UV–vis (CMOS sensor) and NIR (InGaAs diode array sensor). The delay between pump and probe beam for Helios was altered using a mechanical delay stage that has a maximum delay time of around 5.8 ns. For EOS, the delay time between pump and probe is electronically tuned and has a maximum time window of 400 μ s.

2.6. Quasi-Steady-state PIA spectroscopy. Quasi-steady-state PIA measurements were performed with a home-built setup using a 532 nm LED source as pump beam and a Xe-lamp or the white-continuum in EOS setup as probe beam. The pump beam was chopped at a frequency of 500 Hz. The probe beam was collected using a dual detector for UV–vis (CMOS sensor) and NIR (InGaAs diode array sensor).

3. RESULTS AND DISCUSSION

The details for the fabrication of both the conventional and inverted devices are described in the [Experimental Section](#). Note that both device types are fabricated under similar processing conditions, including the same active layer, thickness, ETL, hole transporting layer (HTL) and so forth to make sure the comparison reliable.

Table 1. Device Performance Parameters for BHJ Solar Cells based on DRCN7T:PC₇₁BM (w/w, 1:0.5) with Conventional and Inverted Structures

	V_{oc} (V)	J_{sc} (mA cm ⁻²)	FF	PCE _{ave} (%)	PCE _{max} (%)	R_s Ω cm ²	R_{sh} Ω cm ²
conventional (120 nm)	0.91 ± 0.01	13.07 ± 0.10	0.65 ± 0.02	7.75 ± 0.31	8.06	6.76	1094
inverted (120 nm)	0.90 ± 0.01	14.09 ± 0.19	0.68 ± 0.01	8.60 ± 0.24	8.84	5.10	1113

3.1. Optical Simulation. In order to understand the impact of device structures on the light intensity distribution in the active layer, optical simulations were first performed based on real device conditions using a one-dimensional transfer matrix model (TMM) for both cases.^{54–56} As shown in Figure S-1, the optical simulation shows that the electric field intensity is distributed differently within the active layer for the conventional and inverted devices. Importantly, in the case of inverted structure, this optical simulation predicts an improved absorption, such as 6.3% improved absorption at the maximum absorption (621 nm) position of the donor material, which is expected to increase the short circuit current density (J_{sc}) accordingly. This can be observed more clearly in the simulated exciton generation rates⁵⁷ for both devices shown in Figure 2, which gives the extremal $J_{sc, simu}$ (assuming internal quantum efficiency (IQE) = 100%) of 15.03 and 16.13 mA cm⁻² for the conventional and inverted structure device (as shown in Figure S-2), respectively. Therefore, an improved PCE would be expected for the inverted structure device if other parameters such as open circuit voltage (V_{oc}) and fill factor (FF) could be similar in both cases.

3.2. Electron and Hole Transporting Layers. On the basis of the optical simulation results, we fabricated both conventional and inverted devices with DRCN7T:PC₇₁BM as the active layer (as shown in Figure 1). Considering the complicated preparation process and high post-thermal annealing temperature (varies from 200 to 450 °C in literatures) for sol-gel ZnO,^{9,10,14,28} ZnO NPs were prepared by the direct hydrolysis method,⁵³ and used as the ETL in the inverted structure device (Figures S-3 and S-4). Furthermore, none of any conjugated or nonconjugated polyelectrolyte was used to modify the work function of cathode or ZnO,^{9,11,14} and modified PEDOT:PSS⁵⁸ was used as the HTL, thereby simplifying the device fabrication process.

3.3. Device Performance. The optimized device performance parameters with both conventional and inverted structures under the illumination of AM 1.5G, 100 mW cm⁻² are summarized in Table 1. Figure 3a shows the typical $J-V$ curves of the above optimized devices. As shown in Table 1, the conventional device exhibited a moderate PCE of 8.06%, with V_{oc} = 0.92 V, J_{sc} = 13.07 mA cm⁻² and FF = 0.67. Note that the device with inverted structure exhibited a sharply enhanced PCE to 8.84% with an improved J_{sc} of 14.28 mA cm⁻² and FF of 0.68. To the best of our knowledge, this PCE of 8.84% is the highest efficiency reported for inverted small molecule-based solar cells,^{28,50,52} and is also among the highest efficiencies reported of polymer-based solar cells.^{10,15,17,59} The V_{oc} and FF are identical in both devices, while the J_{sc} for the inverted device shows about 9% increment compared with the conventional device, which is consistent with the optical simulation results discussed above.

As shown in Table 1, the series resistance (R_s) for the conventional and inverted device is 6.76 and 5.10 Ω cm², respectively. Meanwhile, the conventional and inverted devices exhibit similar shunt resistances (R_{sh}) of 1094. and 1113 Ω cm².

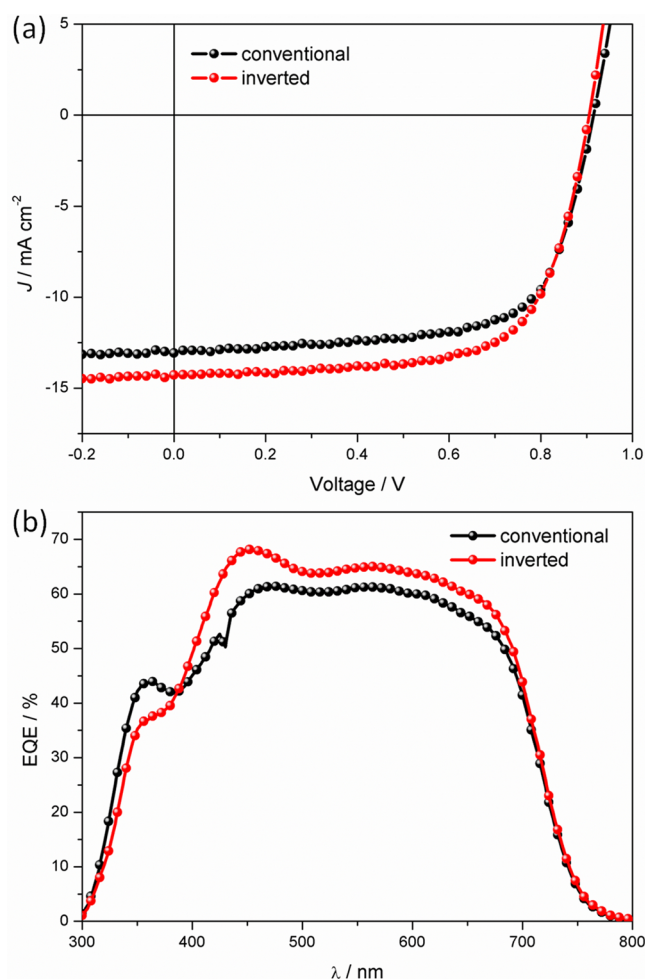


Figure 3. $J-V$ curves (a) and EQE spectra (b) of the conventional device with structure of ITO/PEDOT:PSS/DRCN7T:PC₇₁BM/ZnO NPs/Al and the inverted device with structure of ITO/ZnO NPs/DRCN7T:PC₇₁BM/modified PEDOT:PSS/Ag under simulated 100 mW cm⁻² (AM 1.5G) illumination.

These data are consistent with the comparable FF for the conventional and inverted devices.

The external quantum efficiency (EQE) spectra for the optimized devices based on DRCN7T with conventional and inverted structures are shown in Figure 3b. The inverted structure device exhibits higher photoelectron conversion efficiency from 400 to 700 nm than that of the conventional device, with the highest EQE value reaching 68% at 455 nm, while the conventional device showed a peak EQE of 62% at 470 nm. These results are consistent with the optical simulated real absorptions in the active layer of the corresponding devices (as shown in Figure S-5), and prove that the inverted structure could indeed improve the J_{sc} and therefore the PCE.

3.4. Mechanism Studies. The increased J_{sc} in the inverted structure OPV devices could originate from the reduced nongeminate recombination or the increased absorption of photons, or a combination of both.¹⁵ In order to clarify the

origin of the enhanced J_{sc} , we will investigate the recombination mechanisms for both the conventional and inverted device based on light-intensity-dependent current–voltage experiments,^{27,60,61} photocurrent density–effective voltage analyses,^{60,62} transient absorption measurements^{63,64} and electrical simulations^{65,66} in the following section.

3.4.1. Light-intensity-dependent Current–Voltage Experiments. Analysis of the current density–voltage characteristics at various light intensities could provide important information about the recombination mechanisms in organic solar cells. We measured the J – V curves for both conventional and inverted device under different light intensities from 5 to 100 mW cm^{-2} (as shown in Figure S-6). The normalized photocurrent density for the conventional and inverted devices at different light intensities is shown in Figure S-7, it is found that the charge collection efficiencies remain constant over a wide range of the applied voltages (from short circuit conditions to the maximum power output point) for both devices. This indicates that both the conventional and inverted devices exhibit similar recombination losses under optimized conditions, which are dominated by almost the same first-order recombination from the short-circuit condition to the open-circuit condition.²⁷

The light intensity dependence of the J_{sc} could provide valuable insight into the charge recombination kinetics at short circuit condition. At the short circuit condition, if there is no nongeminate recombination, the J_{sc} should be correlated to the light intensity (P) by eq 1 with $\alpha = 1$,

$$J_{sc} \propto P^\alpha \quad (1)$$

The light intensity dependence of the J_{sc} for the conventional and inverted devices is shown in Figure 4a. The fitted power law yield α for the conventional and inverted devices are 0.967 ± 0.006 and 0.959 ± 0.007 , respectively, which indicates a negligible nongeminate recombination for both conventional and inverted devices.

If the mean effective electron or hole drift length is smaller than the film thickness or the charge carrier mobilities are not balanced in the devices, then the build-up of space charges will arise, and nongeminate recombination will become considerable. When the build-up of space charges reaches a fundamental limit, the photocurrent will have a three-fourth power dependence on light intensity ($\alpha = 3/4$).⁶⁰ On the contrary, when there is no build-up of space charges, suggesting that all the separated charges are collected under perfect conditions, the power law dependence will give a factor of 1.⁶¹ The experimental power law dependence of photocurrent vs incident light intensity is shown in Figure 4, parts b and c, at a high effective voltage ($V_{\text{eff}} = 2$ V), the power exponents (α) for conventional and inverted devices are 0.968 ± 0.007 and 0.962 ± 0.007 , respectively, very close to the perfect conditions. At the short circuit condition, the power exponents for the conventional and inverted device are 0.967 ± 0.006 and 0.963 ± 0.007 . Meanwhile, at the low effective voltage (ca. 0.26 V) corresponding to an external bias of 0.73 V where the maximum power output is observed, the power exponents for conventional and inverted device still exhibit similar and high values of 0.962 ± 0.006 and 0.961 ± 0.006 , respectively. All these suggest little build-up of space charge and similar nongeminate recombination for both conventional and inverted structure devices.

3.4.2. Photocurrent Density-Effective Voltage Analyses. In order to further investigate the causes of the improved J_{sc} in the inverted device over the conventional device, the photocurrent

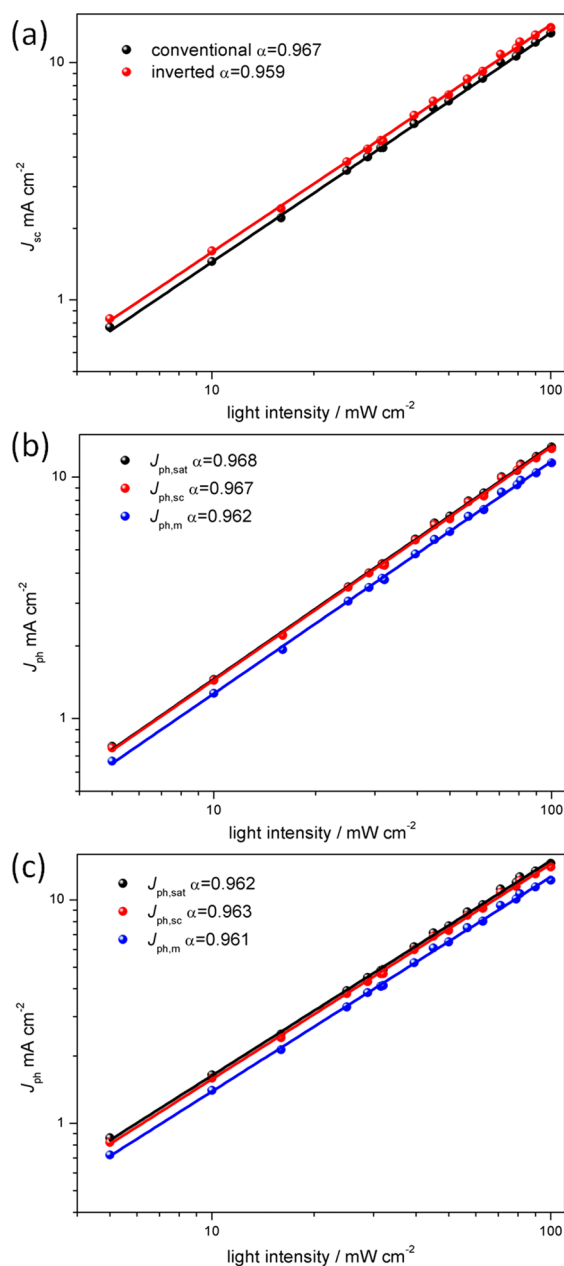


Figure 4. (a) Measured J_{sc} of DRCN7T:PC₇₁BM solar cells with conventional and inverted structure devices plotted against light intensity on a logarithmic scale. The $J_{\text{ph,sat}}$, $J_{\text{ph,sc}}$, $J_{\text{ph,m}}$ plotted against with the light intensity for the conventional device structure (b) and inverted device structure (c).

is plotted as a function of the effective applied voltage (V_{eff}) in a wide reverse bias range under AM 1.5G illumination.^{60,62} As shown in Figure 5a, for both conventional and inverted devices, J_{ph} has a nearly linear dependence on the voltage at the low values of V_{eff} which reaches saturation when the effective voltage V_{eff} arrives at ~ 2 V, suggesting that almost all the photogenerated excitons are dissociated into free carriers and all carriers are collected at the electrodes without nongeminate recombination. With the assumption that all the bound exciton pairs are dissociated in this case, the maximum generation rate of bound exciton pairs per unit volume (G_{max}) and the charge collection efficiency (P_c) for the conventional and inverted devices could be determined. G_{max} was calculated from eq 2,

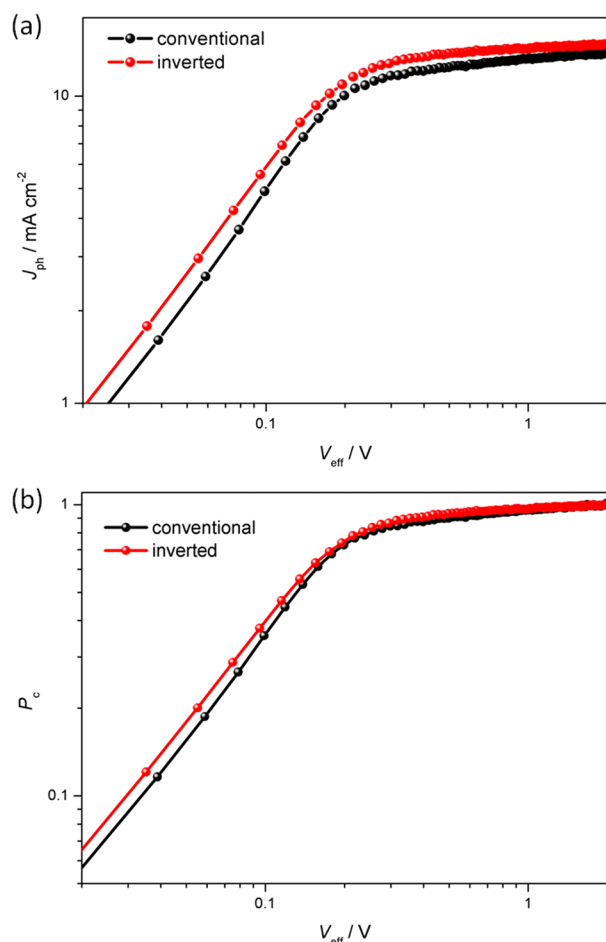


Figure 5. Net photocurrent density (a) and charge collection efficiency (b) versus effective voltage characteristics of the DRCN7T:PC₇₁BM based conventional and inverted devices under constant incident light intensity (AM 1.5G, 100 mW cm⁻²).

$$J_{\text{ph,sat}} = qG_{\text{max}}L \quad (2)$$

where q is the electronic charge and L is the thickness of the active layer (ca. 120 nm for both cases). The values of G_{max} for the inverted device and conventional device are $9.21 \times 10^{27} \text{ m}^{-3} \text{ s}^{-1}$ ($J_{\text{ph,sat}} = 14.76 \text{ mA cm}^{-2}$) and $8.62 \times 10^{27} \text{ m}^{-3} \text{ s}^{-1}$ ($J_{\text{ph,sat}} = 13.81 \text{ mA cm}^{-2}$), respectively. Since G_{max} is related to the maximum absorption of incident photons, the increased G_{max} for the inverted device suggests that better absorption exists, which is also in agreement with the optical simulated $J_{\text{sc,simu}}$ and experimental J_{sc} results as discussed above.

As shown in Figure 5b, the exciton dissociation efficiency could also be obtained at the short circuit condition from eq 3,

$$P_c = J_{\text{ph,sc}}/J_{\text{ph,sat}} \quad (3)$$

At short circuit conditions, the J_{ph} is 95.76% and 96.54% of the saturation current density ($J_{\text{ph,sat}}$) (J_{ph} at $V_{\text{eff}} = 2 \text{ V}$) for the conventional and inverted devices, respectively, which indicates both devices exhibit very high exciton dissociation efficiencies. At the maximal power output condition, $J_{\text{ph}}/J_{\text{ph,sat}}$ for the conventional and inverted device is 81.05% and 83.54%, respectively, further proves that very high charge collection efficiency and less nongeminate recombination loss exists in both device structures.

3.4.3. Transient Absorption Measurements. To elucidate the recombination mechanisms of the conventional and inverted devices, transient absorption (TA) was performed on both devices in a reflection geometry.^{63,64} Figure 6, parts a and b, shows the TA spectra from 5 ns to 1 μs delay for the conventional and inverted structure devices, respectively. The negative part spanning from ~ 600 to $\sim 730 \text{ nm}$ is attributed to the ground state bleaching (GSB) of DRCN7T molecules which is due to the state-filling of the excited states. The long-lived positive shoulder or peak at around 800 and 1150 nm are almost identical to the peaks in the quasi-steady-state photoinduced absorption (PIA) spectra (as shown in Figure S-8). Since the quasi-steady-state PIA monitors the long-lived species and both the 800 and 1150 nm have similar lifetimes of

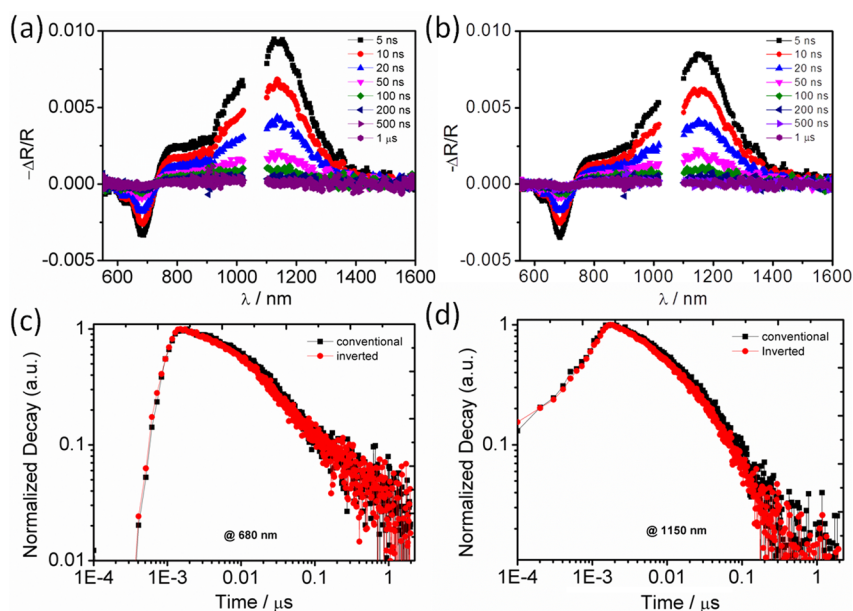


Figure 6. TA spectra (ns– μs) for the conventional (a) and inverted (b) devices, the dynamics at 680 nm (c) and 1150 nm (d) in both devices are overlaid for comparison.

hundreds to microseconds, we ascribe them to the photo-induced absorption of hole polarons in DRCN7T. Figure 6, parts c and d, shows the comparison of GSB and polaron dynamics between conventional and inverted devices monitored at 680 and 1150 nm, respectively. The polarons in both devices have almost the same decay rate indicating that the charge recombination in the conventional and inverted structure devices is invariant. Early time dynamics (fs–ns) also shows there is negligible change in transient dynamics (as shown in Figure S-9). These results further confirmed that the excitation dynamics of DRCN7T:PC₇₁BM was not altered when the device structure was changed. Hence, the enhancement of performance could not be attributed to less recombination loss in inverted device.

3.4.4. Electrical Simulations. The electrical models developed by Nelson et al.^{65,66} were also simulated on both device structures to further clarify the origin of the enhanced J_{sc} . It has been demonstrated by introducing an exponential density of tail trapping states below the band edge of polymer and fullerene, the device performance can be successfully modeled. Charge recombination is considered to be Shockley–Read–Hall (SRH) trap-assisted type recombination that free charges in transporting level annihilate with trapped charges in tail states.^{66,67} The consideration is plausible as we observed a monomolecular recombination as shown in Figure S-7 over the simulated voltage range for both conventional and inverted devices. Considering that the density of state (DOS) width is much narrower in small molecules than in polymers and the high carrier mobility in small molecules,⁶⁸ only fullerene tail trap states are included in the modeling. Nongeminate recombination happens when free holes annihilate with trapped electrons. The absorbed photon flux distribution follows Figure S-2 and multiplies by a reduction factor (due to an overestimated IQE in the electrical field simulation) so that the total absorbed photon is coincident with the maximum current output in experiment. A global fitting was carried out with different incident light intensities for both conventional and inverted devices. The fitting results are shown in Figure S-10 and Table S1 listed the main parameters extracted from the fitting. It is found that with only one set of parameters, both the conventional and inverted devices could be well-fitted based on the simulated absorbed photon flux. This indicates that the performance improvements could only come from a better electrical field distribution profile, where more photons are absorbed in the inverted devices while other factors are hardly affected.

3.5. Device Stability. A preliminary investigation of the long-term stability of the inverted and conventional devices was also carried out. Both devices were encapsulated and stored in the ambient atmosphere (humidity: 65%), their photovoltaic performance was measured periodically by transferring the devices back into the argon-filled glovebox. As shown in Figure S-11, the inverted device showed a remarkable stability with almost no obvious degradation after three months (the PCE is kept at 93% after 103 days). However, the PCE for the conventional device with ZnO NPs as the ETL decreased to 84% after 40 days under the same test conditions, while the conventional device with PFN as the ETL showed a significant decrease (the PCE reduced to 45% after 23 days) under the same test conditions. Also, the light soaking test was performed under the same conditions, and similar results were obtained (as shown in Figure S-12). The PCE for the inverted device was kept almost as a constant after continued illumination for 70

min, while the conventional device employed ZnO NPs as the ETL exhibits about 5% decrease during the same test condition. Therefore, future work should focus on how to enhance the stability of the conventional devices.⁶⁹ On the basis of our results, the SM-OPVs could achieve the comparable stabilities with P-OPVs by using inverted device structures, which exhibit great potential for the future commercial applications.

4. CONCLUSIONS

Using an inverted structure, a PCE of 8.84% has been achieved for solution processed SM-OPV using ZnO NPs as the ETL without any conjugated or nonconjugated polyelectrolytes. The performance improvement for the inverted devices is attributed to the enhanced J_{sc} , which mainly originates from the increased light absorption in the inverted device, rather than the reduced nongeminate recombination compared to the conventional devices fabricated under similar conditions. This is validated from the studies of the optical simulations, light-intensity-dependent current–voltage experiments, photocurrent density-effective voltage analyses, transient absorption measurements and electrical simulations. These results would be helpful for device fabrication and optimization toward future possible commercialization of SM-OPV.

■ ASSOCIATED CONTENT

Supporting Information

The Supporting Information is available free of charge on the ACS Publications website at DOI: 10.1021/acsami.5b05317.

Details of light-intensity-dependent current–voltage experiments, 2D-grazing incidence X-ray diffraction, and so forth (PDF)

■ AUTHOR INFORMATION

Corresponding Authors

*E-mail: tzechien@ntu.edu.sg (T.C.S.).

*E-mail: yschen99@nankai.edu.cn (Y.C.).

Author Contributions

||G.L. and B.W. contributed equally to this work.

Notes

The authors declare no competing financial interest.

■ ACKNOWLEDGMENTS

The authors gratefully acknowledge financial support from the MOST (Grants 2014CB643502 and 2012CB933401), NSFC (Grants 91433101, 51422304, and 51373078), NSF of Tianjin City (Grant 13RCGFGX01121), PCSIRT (IRT1257), the NTU start-up grant M4080514, SPMS collaborative Research Award M4080536, Ministry of Education AcRF Tier 2 grant MOE2013-T2-1-081 and the Singapore National Research Foundation through the Singapore–Berkeley Research Initiative for Sustainable Energy (SinBeRISE) CREATE Programme, and thank beamline BL14B1 (Shanghai Synchrotron Radiation Facility) for providing beam time.

■ REFERENCES

- (1) Beaujuge, P. M.; Fréchet, J. M. J. Molecular Design and Ordering Effects in π -Functional Materials for Transistor and Solar Cell Applications. *J. Am. Chem. Soc.* **2011**, *133*, 20009–20029.
- (2) Cheng, Y. J.; Yang, S. H.; Hsu, C. S. Synthesis of Conjugated Polymers for Organic Solar Cell Applications. *Chem. Rev.* **2009**, *109*, 5868–5923.

- (3) Chen, W.; Nikiforov, M. P.; Darling, S. B. Morphology Characterization in Organic and Hybrid Solar Cells. *Energy Environ. Sci.* **2012**, *5*, 8045–8074.
- (4) Darling, S. B.; You, F. The Case for Organic Photovoltaics. *RSC Adv.* **2013**, *3*, 17633–17648.
- (5) Li, G.; Chu, C.; Shrotriya, V.; Huang, J.; Yang, Y. Efficient Inverted Polymer Solar Cells. *Appl. Phys. Lett.* **2006**, *88*, 253503.
- (6) Yip, H. L.; Jen, A. K. Y. Recent Advances in Solution-Processed Interfacial Materials for Efficient and Stable Polymer Solar Cells. *Energy Environ. Sci.* **2012**, *5*, 5994–6011.
- (7) Søndergaard, R.; Helgesen, M.; Jørgensen, M.; Krebs, F. C. Fabrication of Polymer Solar Cells Using Aqueous Processing for All Layers Including the Metal Back Electrode. *Adv. Energy Mater.* **2011**, *1*, 68–71.
- (8) Şahin, Y.; Alem, S.; de Bettignies, R.; Nunzi, J. M. Development of Air Stable Polymer Solar Cells Using an Inverted Gold on Top Anode Structure. *Thin Solid Films* **2005**, *476*, 340–343.
- (9) Yang, T.; Wang, M.; Duan, C.; Hu, X.; Huang, L.; Peng, J.; Huang, F.; Gong, X. Inverted Polymer Solar Cells With 8.4% Efficiency by Conjugated Polyelectrolyte. *Energy Environ. Sci.* **2012**, *5*, 8208–8214.
- (10) Guo, X.; Zhou, N.; Lou, S. J.; Smith, J.; Tice, D. B.; Hennek, J. W.; Ortiz, R. P.; Navarrete, J. T. L.; Li, S.; Strzalka, J.; Chen, L. X.; Chang, R. P. H.; Facchetti, A.; Marks, T. J. Polymer Solar Cells With Enhanced Fill Factors. *Nat. Photonics* **2013**, *7*, 825–833.
- (11) Chang, J. H.; Wang, H. F.; Lin, W. C.; Chiang, K. M.; Chen, K. C.; Huang, W. C.; Huang, Z. Y.; Meng, H. F.; Ho, R. M.; Lin, H. W. Efficient Inverted Quasi-Bilayer Organic Solar Cells Fabricated by Using Non-Halogenated Solvent Processes. *J. Mater. Chem. A* **2014**, *2*, 13398–13406.
- (12) Tan, Z.; Zhang, W.; Zhang, Z.; Qian, D.; Huang, Y.; Hou, J.; Li, Y. High-Performance Inverted Polymer Solar Cells With Solution-Processed Titanium Chelate As Electron-Collecting Layer on ITO Electrode. *Adv. Mater.* **2012**, *24*, 1476–1481.
- (13) Chen, S.; Small, C. E.; Amb, C. M.; Subbiah, J.; Lai, T. h.; Tsang, S. W.; Manders, J. R.; Reynolds, J. R.; So, F. Inverted Polymer Solar Cells With Reduced Interface Recombination. *Adv. Energy Mater.* **2012**, *2*, 1333–1337.
- (14) Cheng, Y. J.; Hsieh, C. H.; He, Y.; Hsu, C. S.; Li, Y. Combination of Indene-C₆₀ Bis-Adduct and Cross-Linked Fullerene Interlayer Leading to Highly Efficient Inverted Polymer Solar Cells. *J. Am. Chem. Soc.* **2010**, *132*, 17381–17383.
- (15) He, Z.; Zhong, C.; Su, S.; Xu, M.; Wu, H.; Cao, Y. Enhanced Power-Conversion Efficiency in Polymer Solar Cells Using an Inverted Device Structure. *Nat. Photonics* **2012**, *6*, 593–597.
- (16) Li, C. Z.; Chang, C. Y.; Zang, Y.; Ju, H. X.; Chueh, C. C.; Liang, P. W.; Cho, N.; Ginger, D. S.; Jen, A. K. Y. Suppressed Charge Recombination in Inverted Organic Photovoltaics Via Enhanced Charge Extraction by Using a Conductive Fullerene Electron Transport Layer. *Adv. Mater.* **2014**, *26*, 6262–6267.
- (17) Liao, S. H.; Jhuo, H. J.; Cheng, Y. S.; Chen, S. A. Fullerene Derivative-Doped Zinc Oxide Nanofilm As the Cathode of Inverted Polymer Solar Cells With Low-Bandgap Polymer (PTB7-Th) for High Performance. *Adv. Mater.* **2013**, *25*, 4766–4771.
- (18) Kong, J.; Hwang, I. W.; Lee, K. Top-Down Approach for Nanophase Reconstruction in Bulk Heterojunction Solar Cells. *Adv. Mater.* **2014**, *26*, 6275–6283.
- (19) Liu, Y.; Zhao, J.; Li, Z.; Mu, C.; Ma, W.; Hu, H.; Jiang, K.; Lin, H.; Ade, H.; Yan, H. Aggregation and Morphology Control Enables Multiple Cases of High-efficiency Polymer Solar Cells. *Nat. Commun.* **2014**, *5*, 5293–5300.
- (20) Walker, B.; Kim, C.; Nguyen, T. Q. Small Molecule Solution-Processed Bulk Heterojunction Solar Cells. *Chem. Mater.* **2011**, *23*, 470–482.
- (21) Mishra, A.; Bauerle, P. Small Molecule Organic Semiconductors on the Move: Promises for Future Solar Energy Technology. *Angew. Chem., Int. Ed.* **2012**, *51*, 2020–2067.
- (22) Lin, Y.; Li, Y.; Zhan, X. Small Molecule Semiconductors for High-Efficiency Organic Photovoltaics. *Chem. Soc. Rev.* **2012**, *41*, 4245–4272.
- (23) Chen, Y.; Wan, X.; Long, G. High Performance Photovoltaic Applications Using Solution-Processed Small Molecules. *Acc. Chem. Res.* **2013**, *46*, 2645–2655.
- (24) Coughlin, J. E.; Henson, Z. B.; Welch, G. C.; Bazan, G. C. Design and Synthesis of Molecular Donors for Solution-Processed High-Efficiency Organic Solar Cells. *Acc. Chem. Res.* **2014**, *47*, 257–270.
- (25) Liu, J.; Walker, B.; Tamayo, A.; Zhang, Y.; Nguyen, T. Q. Effects of Heteroatom Substitutions on the Crystal Structure, Film Formation, and Optoelectronic Properties of Diketopyrrolopyrrole-Based Materials. *Adv. Funct. Mater.* **2013**, *23*, 47–56.
- (26) Nikiforov, M. P.; Lai, B.; Chen, W.; Chen, S.; Schaller, R. D.; Strzalka, J.; Maser, J.; Darling, S. B. Detection and Role of Trace Impurities in High-Performance Organic Solar Cells. *Energy Environ. Sci.* **2013**, *6*, 1513–1520.
- (27) Kyaw, A. K. K.; Wang, D. H.; Gupta, V.; Leong, W. L.; Ke, L.; Bazan, G. C.; Heeger, A. J. Intensity Dependence of Current-Voltage Characteristics and Recombination in High-Efficiency Solution-Processed Small-Molecule Solar Cells. *ACS Nano* **2013**, *7*, 4569–4577.
- (28) Kyaw, A. K. K.; Wang, D. H.; Gupta, V.; Zhang, J.; Chand, S.; Bazan, G. C.; Heeger, A. J. Efficient Solution-Processed Small-Molecule Solar Cells With Inverted Structure. *Adv. Mater.* **2013**, *25*, 2397–2402.
- (29) Shin, J.; Kang, N. S.; Kim, K. H.; Lee, T. W.; Jin, J. I.; Kim, M.; Lee, K.; Ju, B. K.; Hong, J. M.; Choi, D. H. J-Aggregation Induced Low Bandgap Anthracene-Based Conjugated Molecule for Solution-Processed Solar Cells. *Chem. Commun.* **2012**, *48*, 8490–8492.
- (30) Rousseau, T.; Cravino, A.; Ripaud, E.; Leriche, P.; Rihn, S.; De Nicola, A.; Ziessel, R.; Roncali, J. A Tailored Hybrid BODIPY-Oligothiophene Donor for Molecular Bulk Heterojunction Solar Cells With Improved Performances. *Chem. Commun.* **2010**, *46*, 5082–5084.
- (31) Shang, H.; Fan, H.; Liu, Y.; Hu, W.; Li, Y.; Zhan, X. A Solution-Processable Star-Shaped Molecule for High-Performance Organic Solar Cells. *Adv. Mater.* **2011**, *23*, 1554–1557.
- (32) Lee, O. P.; Yiu, A. T.; Beaujuge, P. M.; Woo, C. H.; Holcombe, T. W.; Millstone, J. E.; Douglas, J. D.; Chen, M. S.; Fréchet, J. M. Efficient Small Molecule Bulk Heterojunction Solar Cells With High Fill Factors Via Pyrene-Directed Molecular Self-Assembly. *Adv. Mater.* **2011**, *23*, 5359–5363.
- (33) Bürckstümmer, H.; Tulyakova, E. V.; Deppisch, M.; Lenze, M. R.; Kronenberg, N. M.; Gsänger, M.; Stolte, M.; Meerholz, K.; Würthner, F. Efficient Solution-Processed Bulk Heterojunction Solar Cells by Antiparallel Supramolecular Arrangement of Dipolar Donor-Acceptor Dyes. *Angew. Chem., Int. Ed.* **2011**, *50*, 11628–11632.
- (34) Fitzner, R.; Mena-Osteritz, E.; Mishra, A.; Schulz, G.; Reinold, E.; Weil, M.; Körner, C.; Ziehlke, H.; Elschner, C.; Leo, K.; Riede, M.; Pfeiffer, M.; Urich, C.; Bäuerle, P. Correlation of π -Conjugated Oligomer Structure With Film Morphology and Organic Solar Cell Performance. *J. Am. Chem. Soc.* **2012**, *134*, 11064–11067.
- (35) Kan, B.; Zhang, Q.; Li, M.; Wan, X.; Ni, W.; Long, G.; Wang, Y.; Yang, X.; Feng, H.; Chen, Y. Solution-Processed Organic Solar Cells Based on Dialkylthiol-Substituted Benzodithiophene Unit With Efficiency near 10%. *J. Am. Chem. Soc.* **2014**, *136*, 15529–15532.
- (36) Zhou, J.; Zuo, Y.; Wan, X.; Long, G.; Zhang, Q.; Ni, W.; Liu, Y.; Li, Z.; He, G.; Li, C.; Kan, B.; Li, M.; Chen, Y. Solution-Processed and High-Performance Organic Solar Cells Using Small Molecules With a Benzodithiophene Unit. *J. Am. Chem. Soc.* **2013**, *135*, 8484–8487.
- (37) Long, G.; Wan, X.; Kan, B.; Hu, Z.; Yang, X.; Zhang, Y.; Zhang, M.; Wu, H.; Huang, F.; Su, S.; Cao, Y.; Chen, Y. Impact of the Electron-Transport Layer on the Performance of Solution-Processed Small-Molecule Organic Solar Cells. *ChemSusChem* **2014**, *7*, 2358–2364.
- (38) Wei, G.; Wang, S.; Sun, K.; Thompson, M. E.; Forrest, S. R. Solvent-Annealed Crystalline Squaraine:PC₇₀BM (1:6) Solar Cells. *Adv. Energy Mater.* **2011**, *1*, 184–187.

- (39) Liu, Y.; Yang, Y.; Chen, C. C.; Chen, Q.; Dou, L.; Hong, Z.; Li, G.; Yang, Y. Solution-Processed Small Molecules Using Different Electron Linkers for High-Performance Solar Cells. *Adv. Mater.* **2013**, *25*, 4657–4662.
- (40) Wang, H.; Liu, F.; Bu, L.; Gao, J.; Wang, C.; Wei, W.; Russell, T. P. The Role of Additive in Diketopyrrolopyrrole-Based Small Molecular Bulk Heterojunction Solar Cells. *Adv. Mater.* **2013**, *25*, 6519–6525.
- (41) Shen, S.; Jiang, P.; He, C.; Zhang, J.; Shen, P.; Zhang, Y.; Yi, Y.; Zhang, Z.; Li, Z.; Li, Y. Solution-Processable Organic Molecule Photovoltaic Materials With Bithienyl-Benzodithiophene Central Unit and Indenedione End Groups. *Chem. Mater.* **2013**, *25*, 2274–2281.
- (42) Huang, J.; Zhan, C.; Zhang, X.; Zhao, Y.; Lu, Z.; Jia, H.; Jiang, B.; Ye, J.; Zhang, S.; Tang, A.; Liu, Y.; Pei, Q.; Yao, J. Solution-Processed DPP-Based Small Molecule That Gives High Photovoltaic Efficiency With Judicious Device Optimization. *ACS Appl. Mater. Interfaces* **2013**, *5*, 2033–2039.
- (43) Loser, S.; Bruns, C. J.; Miyauchi, H.; Ortiz, R. o. P.; Facchetti, A.; Stupp, S. I.; Marks, T. J. A Naphthodithiophene-Diketopyrrolopyrrole Donor Molecule for Efficient Solution-Processed Solar Cells. *J. Am. Chem. Soc.* **2011**, *133*, 8142–8145.
- (44) Li, W.; Kelchtermans, M.; Wienk, M. M.; Janssen, R. A. J. Effect of Structure on the Solubility and Photovoltaic Properties of Bis-Diketopyrrolopyrrole Molecules. *J. Mater. Chem. A* **2013**, *1*, 15150–15157.
- (45) Min, J.; Luponosov, Y. N.; Zhang, Z. G.; Ponomarenko, S. A.; Ameri, T.; Li, Y.; Brabec, C. J. Interface Design to Improve the Performance and Stability of Solution-Processed Small-Molecule Conventional Solar Cells. *Adv. Energy Mater.* **2014**, *4*, 1400816–1400824.
- (46) Zhang, Q.; Kan, B.; Liu, F.; Long, G.; Wan, X.; Chen, X.; Zuo, Y.; Ni, W.; Zhang, H.; Li, M. H. Z.; Huang, F.; Cao, Y.; Liang, Z.; Zhang, M.; Thomas, P. R.; Chen, Y. Small-Molecule-Based Solar Cells With Efficiency Over 9%. *Nat. Photonics* **2015**, *9*, 35–41.
- (47) Liu, Y.; Wan, X.; Wang, F.; Zhou, J.; Long, G.; Tian, J.; You, J.; Yang, Y.; Chen, Y. Spin-Coated Small Molecules for High Performance Solar Cells. *Adv. Energy Mater.* **2011**, *1*, 771–775.
- (48) Li, Z.; He, G. R.; Wan, X. J.; Liu, Y. S.; Zhou, J. Y.; Long, G. K.; Zuo, Y.; Zhang, M. T.; Chen, Y. S. Solution Processable Rhodanine-Based Small Molecule Organic Photovoltaic Cells With a Power Conversion Efficiency of 6.1%. *Adv. Energy Mater.* **2012**, *2*, 74–77.
- (49) Long, G.; Wan, X.; Kan, B.; Liu, Y.; He, G.; Li, Z.; Zhang, Y.; Zhang, Y.; Zhang, Q.; Zhang, M.; Chen, Y. Investigation of Quinqueithiophene Derivatives With Different End Groups for High Open Circuit Voltage Solar Cells. *Adv. Energy Mater.* **2013**, *3*, 639–646.
- (50) Lin, H. Y.; Huang, W. C.; Chen, Y. C.; Chou, H. H.; Hsu, C. Y.; Lin, J. T.; Lin, H. W. BODIPY Dyes With β -Conjugation and Their Applications for High-Efficiency Inverted Small Molecule Solar Cells. *Chem. Commun.* **2012**, *48*, 8913–8915.
- (51) Yamamoto, T.; Hatano, J.; Nakagawa, T.; Yamaguchi, S.; Matsuo, Y. Small Molecule Solution-Processed Bulk Heterojunction Solar Cells With Inverted Structure Using Porphyrin Donor. *Appl. Phys. Lett.* **2013**, *102*, 013305.
- (52) Shin, W.; Yasuda, T.; Hidaka, Y.; Watanabe, G.; Arai, R.; Nasu, K.; Yamaguchi, T.; Murakami, W.; Makita, K.; Adachi, C. π -Extended Narrow-Bandgap Diketopyrrolopyrrole-Based Oligomers for Solution-Processed Inverted Organic Solar Cells. *Adv. Energy Mater.* **2014**, *4*, 1400879–1400888.
- (53) Beek, W. J. E.; Wienk, M. M.; Kemerink, M.; Yang, X.; Janssen, R. A. J. Hybrid Zinc Oxide Conjugated Polymer Bulk Heterojunction Solar Cells. *J. Phys. Chem. B* **2005**, *109*, 9505–9516.
- (54) Burkhard, G. F.; Hoke, E. T.; McGehee, M. D. Accounting for Interference, Scattering, and Electrode Absorption to Make Accurate Internal Quantum Efficiency Measurements in Organic and Other Thin Solar Cells. *Adv. Mater.* **2010**, *22*, 3293–3297.
- (55) Pettersson, L. A. A.; Roman, L. S.; Inganäs, O. Modeling Photocurrent Action Spectra of Photovoltaic Devices Based on Organic Thin Films. *J. Appl. Phys.* **1999**, *86*, 487–496.
- (56) Peumans, P.; Yakimov, A.; Forrest, S. R. Small Molecular Weight Organic Thin-film Photodetectors and Solar Cells. *J. Appl. Phys.* **2003**, *93*, 3693–3723.
- (57) Chen, K. S.; Salinas, J. F.; Yip, H. L.; Huo, L.; Hou, J.; Jen, A. K. Y. Semi-Transparent Polymer Solar Cells With 6% PCE, 25% Average Visible Transmittance and a Color Rendering Index Close to 100 for Power Generating Window Applications. *Energy Environ. Sci.* **2012**, *5*, 9551–9557.
- (58) Shi, H.; Liu, C.; Jiang, Q.; Xu, J. Effective Approaches to Improve the Electrical Conductivity of PEDOT:PSS: A Review. *Adv. Electron. Mater.* **2015**, *1*, 1500017–1500032.
- (59) Lu, L.; Xu, T.; Chen, W.; Landry, E. S.; Yu, L. Ternary Blend Polymer Solar Cells With Enhanced Power Conversion Efficiency. *Nat. Photonics* **2014**, *8*, 716–722.
- (60) Blom, P. W. M.; Mihailtchi, V. G. D.; Koster, L. G. J.; Markov, D. G. E. Device Physics of Polymer:Fullerene Bulk Heterojunction Solar Cells. *Adv. Mater.* **2007**, *19*, 1551–1566.
- (61) Lenes, M.; Morana, M.; Brabec, C. J.; Blom, P. W. M. Recombination-Limited Photocurrents in Low Bandgap Polymer/Fullerene Solar Cells. *Adv. Funct. Mater.* **2009**, *19*, 1106–1111.
- (62) Proctor, C. M.; Kim, C.; Neher, D.; Nguyen, T. Q. Nongeminate Recombination and Charge Transport Limitations in Diketopyrrolopyrrole-Based Solution-Processed Small Molecule Solar Cells. *Adv. Funct. Mater.* **2013**, *23*, 3584–3594.
- (63) Marsh, R. A.; Hodgkiss, J. M.; Friend, R. H. Direct Measurement of Electric Field-Assisted Charge Separation in Polymer:Fullerene Photovoltaic Diodes. *Adv. Mater.* **2010**, *22*, 3672–3676.
- (64) Marsh, R. A.; Hodgkiss, J. M.; bert-Seifried, S.; Friend, R. H. Effect of Annealing on P3HT:PCBM Charge Transfer and Nanoscale Morphology Probed by Ultrafast Spectroscopy. *Nano Lett.* **2010**, *10*, 923–930.
- (65) Kirchartz, T.; Pieters, B. E.; Kirkpatrick, J.; Rau, U.; Nelson, J. Recombination via Tail States in Polythiophene: Fullerene Solar Cells. *Phys. Rev. B: Condens. Matter Mater. Phys.* **2011**, *83*, 115209.
- (66) MacKenzie, R. C. I.; Shuttle, C. G.; Chabiny, M. L.; Nelson, J. Extracting Microscopic Device Parameters From Transient Photocurrent Measurements of P3HT:PCBM Solar Cells. *Adv. Energy Mater.* **2012**, *2*, 662–669.
- (67) Shockley W, R. WT. Statistics of the Recombinations of Holes and Electrons. *Phys. Rev.* **1952**, *87*, 835–842.
- (68) Zhong, C.; Huang, F.; Cao, Y.; Moses, D.; Heeger, A. J. Role of Localized States on Carrier Transport in Bulk Heterojunction Materials Comprised of Organic Small Molecule Donors. *Adv. Mater.* **2014**, *26*, 2341–2345.
- (69) Li, C. Z.; Chueh, C. C.; Yip, H. L.; O' Malley, K. M.; Chen, W. C.; Jen, A. K. Effective Interfacial Layer to Enhance Efficiency of Polymer Solar Cells Via Solution-Processed Fullerene-Surfactants. *J. Mater. Chem.* **2012**, *22*, 8574–8578.